Nanoscale

PAPER

View Article Online
View Journal | View Issue

Cite this: *Nanoscale*, 2023, **15**, 18667

Nanoarchitectonics composite hydrogels with high toughness, mechanical strength, and self-healing capability for electrical actuators with programmable shape memory properties†

Yanqing Wang, Pengcheng Li, Shuting Cao, Yuetao Liu and Chuanhui Gao *

Hydrogel materials show promise in various fields, including flexible electronic devices, biological tissue engineering and wound dressing. Nevertheless, the inadequate mechanical properties, recovery performance, and self-healing speed still constrain the development of intelligent hydrogel materials. To tackle these challenges, we designed a composite hydrogel with high mechanical strength, rapid self-recovery and efficient self-healing ability based on multiple synergistic effects. With the synergistic effect of hydrogen bonds, metal coordination bonds and electrostatic interaction, the synthesized hydrogel could reach a maximum tensile strength of 6.2 MPa and a toughness of 50 MJ m^{-3}. The interaction between the weak polyelectrolyte polyethyleneimine and polyacrylic acid aided in improving the elasticity of the hydrogel, thereby endowing it with prompt self-recovery attributes. The multiple reversible effects also endowed the hydrogel with excellent self-healing ability, and the fractured hydrogel could achieve 95% self-healing within 4 h at room temperature. By the addition of glycerol, the hydrogel could also cope with a variety of extreme environments in terms of moisture retention (12 h, maintaining 80% of its water content) and freeze protection (−36.8 °C) properties. In addition, the composite hydrogels applied in the field of shape memory possessed programmable and reversible shape transformation properties. The polymer chains were entangled at high temperatures to achieve shape fixation, and shape memory was eliminated at low temperatures, which allowed the hydrogels to be reprogrammed and achieve multiple shape transitions. In addition, we also assemble composite hydrogels as actuators and robotic arms for intelligent applications.

Received 22nd July 2023,
Accepted 24th October 2023

DOI: 10.1039/d3nr03578f

rsc.li/nanoscale

1 Introduction

Hydrogels, with a flexible three-dimensional mesh structure, possess a wide range of applications in soft robotics,[1–3] electronic sensing,[4–6] and tissue engineering.[7–9] However, the development of hydrogel materials with high toughness, high mechanical strength and excellent self-healing ability has been attracting the attention of researchers. Many scientists have focused on designing specific structures (*e.g.*, dual-network hydrogels) and adding nanomaterials.[10–12] For example, Wu's team developed a double-ion cross-linked hydrogel with a tensile strength of up to 3.2 MPa.[13] However, for highly ductile and mechanically strong hydrogels, fast self-recovery is critical.[14,15] He's team created a class of composite hydrogels with a triple network by combining chemical and physical cross-linking.[16] The resulting hydrogels, PVA/CS/PAAm, possessed a tensile strength of 2.10 MPa and an elongation at break of 510%. However, despite combining the advantages of each network structure for compression properties, the recovery properties were lacking. Mo *et al.* developed a hydrogel by utilizing tannic acid-enabled dynamic interaction (TEDI), which exhibited impressive qualities including high adhesion, super-stretchability and self-healing capacity. This produced material boasts incredible tensile strength with a maximum strain value of up to 7500%. However, fatigue resistance and self-healing capabilities were often insufficient, which restricted its potential applications.[17] This is because excellent self-recovery reduces the degradation of mechanical properties arising from the long-term operation of the hydrogel. The self-recovery of the material could be effectively improved by introducing reversible non-covalent interactions within the system;[18–20] however, it still takes a long time for high toughness hydrogels to recover completely.

Environmental tolerance and longevity often limit the practical application of hydrogels. As pure water constitutes the majority of hydrogel solvents, the material inevitably freezes at

College of Chemical Engineering, Qingdao University of Science and Technology, Qingdao 266042, China. E-mail: gaochuanhui@qust.edu.cn; Tel: +86 0532-84023170

† Electronic supplementary information (ESI) available. See DOI: https://doi.org/10.1039/d3nr03578f

sub-zero temperatures and its effectiveness is hindered due to water evaporation.[21,22] These challenges consequently affect the application of hydrogel materials. The addition of organic solvents could significantly improve this deficiency. The recently reported mechanisms of self-healing hydrogels are mainly based on hydrogen bonding interactions, Schiff base reactions, host–guest interactions, ionic interactions, *etc.*[23–26] Jiang's group synthesized a hydrogel based on a polyvinyl alcohol hydrogen bonding network, and the hydrogel exhibited rapid self-healing ability by the combined action of numerous hydrogen bonding networks.[27] Zhang's group explored a rapid self-healing hydrogel cross-linked by acylhydrazone bonds.[28] However, the mechanical properties of these hydrogels are frequently inadequate, rendering them challenging to utilize for prolonged periods.[29] Therefore, it is still a challenge to explore new strategies to synthesize hydrogels that combine mechanical properties, efficient self-healing properties and environmental tolerance.

Based on the above challenges, we synthesized a composite hydrogel with multiple synergistic interactions based on hydrogen bonds, metal–ligand bonds and electrostatic interactions. Significantly, the composite hydrogel exhibited an excellent tensile strength of 6.2 MPa and a toughness of 50 MJ m^{-3}, while the fractured hydrogel could reach a self-healing rate of 95% within 4 h. The mechanical properties of the composite hydrogel were modulated using hydrogen bonds, metal–ligand bonds and electrostatic interactions, and the effects of different amounts of polyethyleneimine and glycerol on the toughness and fatigue resistance of the hydrogel were explored. The incorporation of glycerol permitted the hydrogel to hold 80% of its water content for up to 12 h. Simultaneously, the potent hydrogen bonds between the glycerol and water molecules endow the substance with exceptional frost protection, enabling it to preserve its initial condition at −36.8 °C. In addition, the composite hydrogel was made into a shape memory material due to its sensitivity to temperature. The reversible shape transformation properties at different temperatures enable the material to achieve programmable effects, a discovery that sheds light on the development of future smart devices.

2 Experimental section

2.1 Materials

Acrylic acid (AAc, 99%) was used as received from Shanghai Macklin Biochemical Co., Ltd. Zirconyl chloride octahydrate ($ZrOCl_2{\cdot}8H_2O$, AR, 99%), branched polyethyleneimine (PEI, M_w ~25 000), glycerol (Gly, AR, ≥99.5%) and 2,2′-azobis(2-methylpropionamidine) dihydrochloride were purchased from Aladdin Chemical Reagent Co., Ltd (China). All experiments involved used deionized water.

2.2 Synthesis of PAEG-Zr^{4+} hydrogels

First, deionized water and acrylic acid (AAc) with various concentrations of Zr^{4+} were combined in a three-necked flask and stirred until a homogeneous mixture was obtained. The photoinitiator was then added to the mixture and thoroughly mixed. Air bubbles were eliminated using ultrasound, and the prepolymerized solution was moved to a glass container. Polymerisation was initiated under UV light to produce the hydrogels, denoted as PA-Zr_x^{4+} (x = 0.5 mol L^{-1}, 1 mol L^{-1}, 1.5 mol L^{-1}, and 2 mol L^{-1}).

The required quantities of acrylic acid (AAc), glycerol (Gly), zirconium chloride octahydrate (Zr^{4+}) and water were added to a three-necked flask, and the prepolymerisation solution was stirred until it was mixed homogeneously. The photoinitiator was subsequently added to the solution and stirred until it was homogeneously dispersed. Air bubbles were removed by sonication, and the resulting mixture was injected into tailored glass vessels. The prepolymerisation solution was subjected to 60 seconds of UV light irradiation at a wavelength of 365 nm in glassware to obtain the glycerol-based hydrogels, denoted as PAG_y-Zr^{4+} (y = 5 wt%, 10 wt%, 15 wt%, and 20 wt%).

Then branched polyethyleneimine (PEI) was added on the basis of the above steps to obtain hydrogels with different PEI contents, denoted as PAE_zG-Zr^{4+}hydrogels (z = 1 wt%, 3 wt%, 5 wt%, 7 wt%, 9 wt% and 11 wt%).

Table S1 and S2 in the ESI† demonstrate the addition of the experimental raw materials. The reaction vessels made of glass were constructed by using glass plates and silica spacers with a thickness of 0.2 mm.

For the purpose of testing the antifreeze and moisturizing properties, we have labelled the control hydrogel without glycerol as PAE-Zr^{4+}.

2.3. Characterization

Fourier transform infrared (FT-IR) spectra of the different products were recorded on a FT-IR spectrometer (Nicolet IS10, Thermo-Nicolet). The spectra were recorded in the wave number range of 500–4000 cm^{-1}. The resolution of the spectrometer was 2 cm^{-1} Raman curves were recorded using a Raman spectrometer (LabRAM HR, HORIBA Scientific) at 532 nm. The transmittance of hydrogels was measured on a UV-vis spectrophotometer (Agilent Technologies, Cary 5000) with a scanning range of 400–800 nm. The microstructures of hydrogels were photographed using a scanning electron microscope (Hitachi, SU8010). The hydrogel chemical structure was characterized by X-ray photoelectron spectroscopy (XPS, ESCALAB XI+).

The mechanical properties and loading–unloading curves were tested at room temperature using a universal testing machine (CMT4204, Meisite) with a stretching speed of 50 mm min^{-1}. The hydrogels used for testing were standard dumbbell splines (25 mm × 3 mm × 1 mm). The toughness of the material was obtained by calculating the area of integration under the stress–strain curve. The Young's modulus of the material was calculated at a slope of the curve in the strain range of 0–5%. For the purpose of testing the fatigue resistance of the hydrogels, the testing samples were initially stretched to a static tensile strain ranging from 100% to 500%,

before being unloaded. To examine the recuperation capabilities of the hydrogels, the test samples underwent initial stretching to 500% of the static tensile strain and were maintained for varying durations before being released from the load. The dissipation energy was obtained by calculating the area of the cyclic stretching curve.

The self-healing process of the hydrogel at the microscopic level was accomplished using a stereomicroscope (Leica M80, Leica). The self-healing properties of the hydrogel were characterized using a universal testing machine and the self-healing efficiency (SE) was defined by the following equation:

$$SE = \frac{\varepsilon_h}{\varepsilon_0} \times 100\% \quad (1)$$

where ε_0 and ε_h are the strains before and after self-healing.

The low temperature properties of the hydrogels were characterized using a differential scanning calorimeter (DSC 204 F1, Netzsch). The test temperature range was set to −100–20 °C with a heating rate of 50 °C min^{-1}. The mechanical properties at low temperatures were obtained using a universal testing machine. The moisture retention performance test results were acquired by subjecting the PAEG-Zr^{4+} and control hydrogels to varying durations of exposure to air.

The actuation behavior of the hydrogel was determined using a custom device through an electric field. For testing purposes, the stained hydrogel was positioned at the center of an electric field comprising a sodium sulphate solution. Different voltages were then employed to drive the hydrogel samples. The actuation behavior was recorded every 10 seconds and the sample bending angle was the tilt angle at which the hydrogel bends from its initial position.

3 Results and discussion

3.1 Structure and the network of PAEG-Zr^{4+} hydrogels

As shown in Scheme 1 and Fig. S1,† the PAEG-Zr^{4+} hydrogel was prepared by a simple one-pot method. The homogeneous prepolymer solution containing branched polyethyleneimine (PEI), acrylic acid (AAc), glycerol (Gly), zirconyl chloride octahydrate (Zr^{4+}), a photoinitiator and water was dispersed in a glass vessel, which was subjected to UV light irradiation to initiate polymerization. Metal coordination between Zr^{4+} and carboxyl groups in the reaction-produced polymer network and the electrostatic interactions between the carboxyl groups and the protonated amine groups of PEI are the foremost driving forces for hydrogel synthesis. The prepared hydrogel possessed excellent mechanical properties and self-healing characteristics under the further interlocking of multiple synergistic interactions. Furthermore, the introduction of glycerol endowed the hydrogel with excellent antifreeze and moisturizing properties, which allowed the material to be in working condition for a long time.

To demonstrate the successful synthesis of the material, the following tests were used to characterize the structure of the composite hydrogel. The FT-IR patterns of PA-Zr^{4+}, PAG-Zr^{4+} and PAEG-Zr^{4+} hydrogels are shown in Fig. 1a. We conclude that the characteristic peaks of deprotonated carboxylic acid groups at 1383 cm^{-1} and 1390 cm^{-1} appeared in the FT-IR spectra of the PAG-Zr^{4+} and PAEG-Zr^{4+} hydrogels. Meanwhile, the characteristic peak of the protonated amine group at 2870 cm^{-1} was detected in the FT-IR spectrum of the PAEG-Zr^{4+} hydrogel. The above results demonstrated the existence of electrostatic interactions in the polymer network.[30,31] Moreover, the formation of metal-coordination complexes was characterized by Raman and XPS. As demonstrated in Fig. 1b,

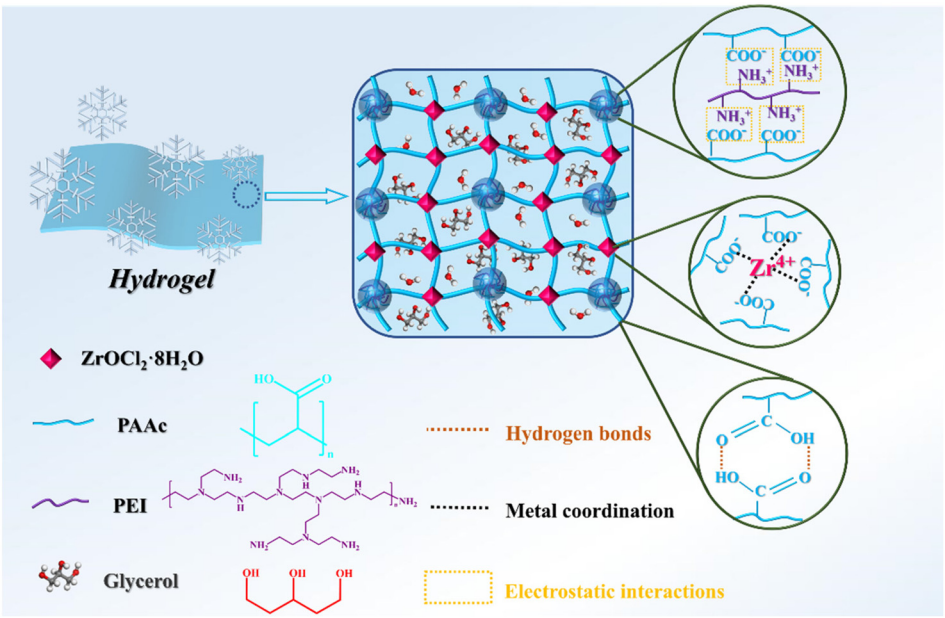

Scheme 1 Schematic diagram of the structural network of the hydrogels.

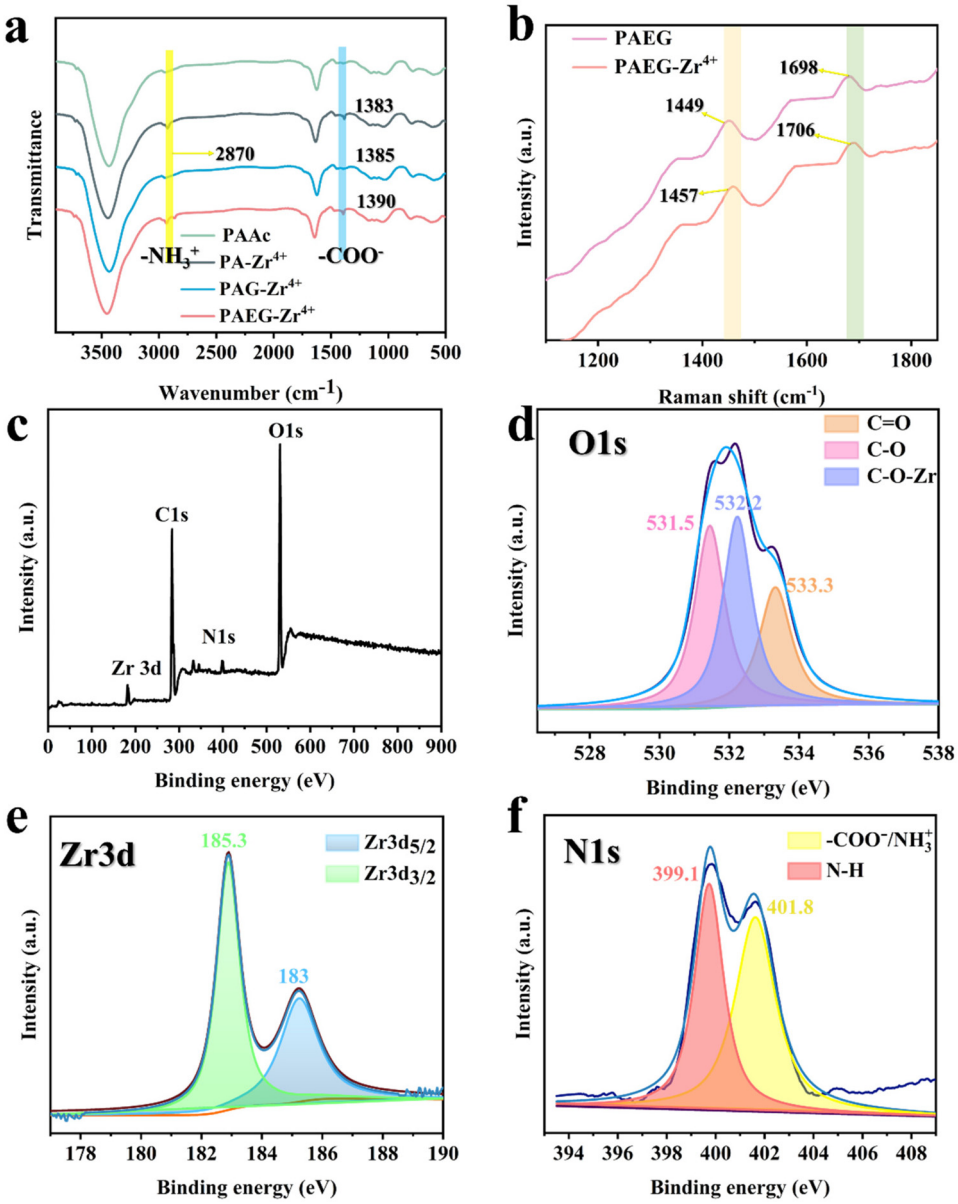

Fig. 1 (a) FT-IR spectra of the PAAc, PA-Zr^{4+}, PAE-Zr^{4+} and PAEG-Zr^{4+} hydrogels. (b) Raman spectra of the PAEG and PAE-Zr^{4+} hydrogels. (c) XPS survey and (d) O 1s XPS spectra of the hydrogels. (e) Zr 3d and (f) N 1s XPS spectra of the hydrogels.

the Raman spectra of the PAEG-Zr^{4+} hydrogels exhibit a shift in the peaks of the deprotonated carboxylic acid groups from 1451 and 1695 to 1457 and 1706 cm^{-1}. This indicated the formation of carboxylic acid groups with Zr^{4+} complexes in comparison with the PAEG hydrogels. Fig. 1c–f show the XPS spectra of the PAEG-Zr^{4+} hydrogels. The O 1s spectra exhibit peaks at binding energies of 533.3 and 531.5 eV, associated with C═O and C–O, respectively, consistent with the PAEG hydrogel test curves (Fig. S2a†). The additional peak observed at 532.2 is attributed to C–O–Zr, signifying the formation of metal coordination bonds.[32] Additionally, the Zr 3d energy spectrum reveals two binding energies at 185.3 and 183 eV, indicating that the metal formed a robust complex with the carboxyl group (Fig. 1e). In contrast to the N 1s spectrum in the PAEG hydrogels (Fig. S2b†), there is a peak at 401.8 eV, which is attributed to the electrostatic interaction between the protonated amine group and the deprotonated carboxyl group.[33]

3.2 Excellent mechanical performance

The resulting multiple synergistic interactions played an important role in the mechanical properties of the PAEG-Zr^{4+} hydrogels. Firstly, we investigated the mechanical strength of the hydrogels with different metal ion concentrations. As shown in Fig. S3,† the stress and strain of the hydrogels increased to different degrees with the increase of Zr^{4+} concen-

tration. At a Zr^{4+} concentration of 1.5 mol L^{-1}, the stress could reach 1.3 MPa, which was rare in hydrogel materials. However, with the further increase of concentration, the increase of the internal cross-linked network rather weakened the mechanical properties. Due to an increase in the concentration of metal ions, the polymer network became overly crosslinked. Consequently, the polymer chain segments experienced a decrease in their degree of freedom, which limited their mobility within the hydrogel network. This process led to a fall in the mechanical properties of the hydrogels.[32,34] Therefore, we chose 1.5 mol L^{-1} metal ion hydrogels for the next study. It has been reported that glycerol, as an organic solvent, could impart antifreeze and moisturizing properties to materials on the one hand and eventually improve the toughness and strength of the hydrogels on the other hand.[35] Therefore, different contents of glycerol were added to adjust the mechanical properties of the composite hydrogel. As shown in Fig. S4a and b,† with the increase of glycerol content (0–15 wt%), the PAEG hydrogels were improved to different degrees in terms of stress, strain and toughness. When the amount of glycerol added was 20 wt%, the mechanical properties of the hydrogels decreased, which may be due to the weakening of intermolecular interactions by excess glycerol.[36] Therefore, we selected PAG-Zr^{4+} hydrogels, containing 15% glycerol content, for further study. As shown in Fig. 2a and b, the PAEG-Zr^{4+} hydrogels could easily lift a 3 kg dumbbell and stretch or twist it arbitrarily. Subsequently, we also investigated the effect of different PEI contents on the mechanical properties of the hydrogels (Fig. 2b). With the increase of PEI content, the stress value increased from 4 MPa to 6.2 MPa, and the strain also increased significantly (1670%). Meanwhile, the corresponding toughness and Young's modulus were calculated as shown in Fig. 2c. The superior toughness of the hydrogels had a value of 50 MJ m^{-3}, which was extremely infrequent in hydrogel materials. The superior strength and toughness of the composite hydrogels are attributed to the synergistic effect between hydrogen bonding, metal–ligand interactions and electrostatic interactions (Scheme 1). On the one hand, the elasticity of the hydrogel could be enhanced between the polyacrylic acid and the weak polyelectrolyte PEI with an opposite charge.[37] Composite hydrogels with nanostructures usually possess excellent mechanical properties (Fig. S5a†). The presence of Zr^{4+} facilitates the formation of a denser nanoscale network structure in the PAEG-Zr^{4+} hydrogels. The metal ions act as cross-linking agents and effectively dissipate the external work of unlinking during the stretching process of the metal–ligand bonds, resulting in excellent mechanical properties.[38] At the same time, the formation of metal complexes by uniformly dis-

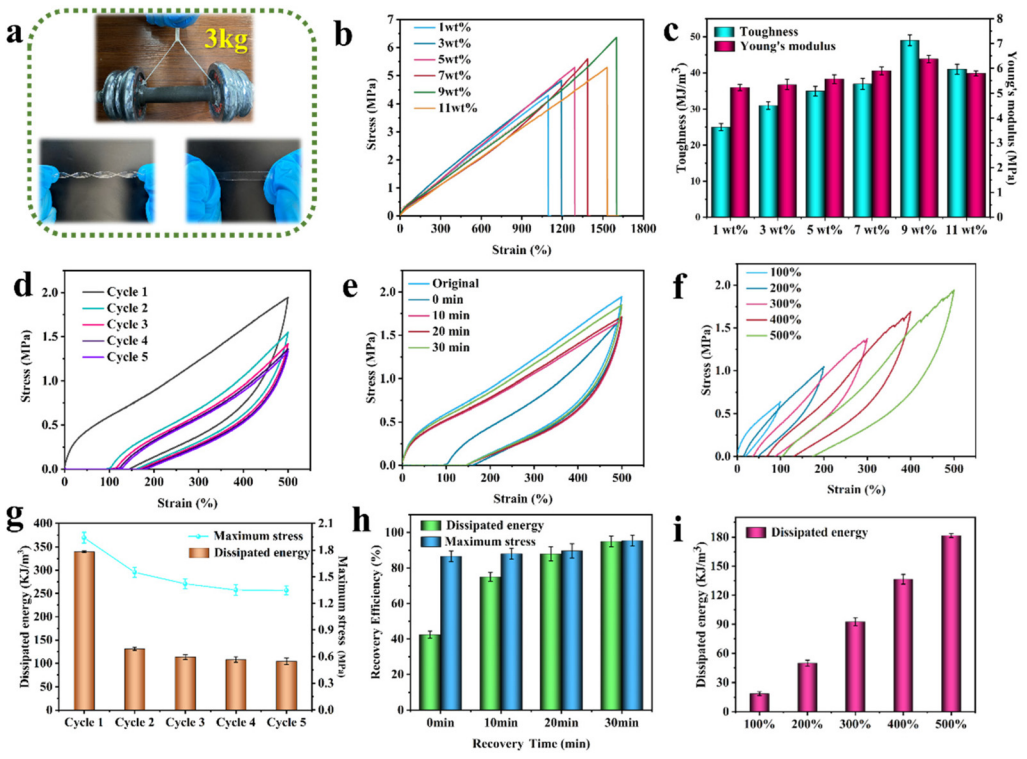

Fig. 2 (a) Digital photos of the hydrogel lifting a dumbbell, twisting and stretching. (b) Stress–strain curves of hydrogels with different ratios of PEI. (c) Toughness and Young's modulus values obtained from the stress–strain curves of PAEG-Zr^{4+} hydrogels. (d) Five continuous tension and relaxation cycles of the PAEG-Zr^{4+} hydrogels. (e) Self-recovery properties of the hydrogels at different resting times. (f) 100–500% cyclic tensile increasing curves of hydrogels. (g) Dissipation energy and maximum stress values of PAEG-Zr^{4+} hydrogels in five cycle tensile tests. (h) Dissipation energy and maximum stress of PAEG-Zr^{4+} hydrogels at different recovery times. (i) Dissipation energy of PAEG-Zr^{4+} hydrogels in tensile tests with different strain cycles.

tributed metal ions (Fig. S5b†) could contribute to the enhancement of the crosslink density of the polymer network, thus further enhancing their mechanical properties.[32,39] Notably, our synthesized hydrogels were highly transparent and could achieve UV transmission rates of over 95% (Fig. S6a†). Based on the above findings, PAEG-Zr^{4+} hydrogels with a PEI content of 9 wt% were used as research subjects for subsequent experiments. For the purpose of discussion, we refer to the hydrogel containing 15 wt% glycerol and 9 wt% PEI as the PAEG-Zr^{4+} hydrogel.

Rapid recovery and fatigue resistance are critical in the practical application of the material. To confirm the rapid fracture and reconstruction behavior of reversible bonds in the polymer network, the PAEG-Zr^{4+} hydrogels were first subjected to five cycles of tensile tests. Fig. 2d and g exhibited five successive loading–unloading cycle curves of PAEG-Zr^{4+} hydrogels and the corresponding dissipation energy. We could see a decrease in the mechanical strength and hysteresis line of the hydrogel during the second cycle. This phenomenon was attributed to the fact that the polymer network sacrificed internally during the first stretching cycle could not be recovered immediately. In the subsequent cycling experiments, the cycling curves exhibited almost overlapping trends, indicating that the PAEG-Zr^{4+} hydrogels had excellent fatigue resistance. In addition, cyclic stretching experiments with different relaxation times were performed to examine the self-recovery of the hydrogels. As shown in Fig. 2e and h, the hysteresis loops of the hydrogel for immediate cyclic stretching were significantly smaller than those of the original hydrogel. The maximum stress and dissipation energy of the hydrogel gradually recov-

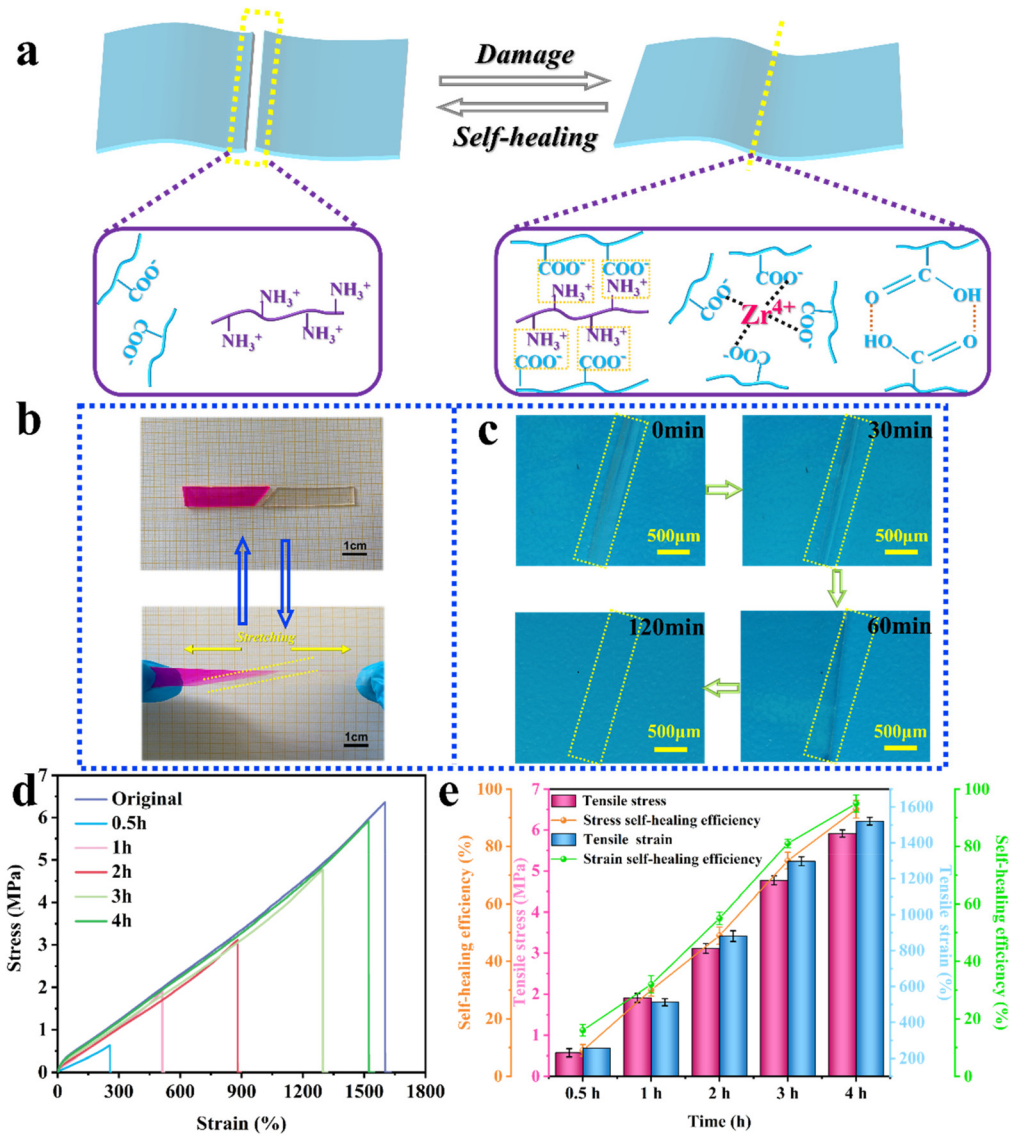

Fig. 3 (a) Self-healing mechanism diagram of PAEG-Zr^{4+} hydrogels. (b) Digital photographs of self-healing hydrogels undergoing stretching. (c) Optical microscopy images of the self-healing process of PAEG-Zr^{4+} hydrogels. (d) Stress–strain curves of PAEG-Zr^{4+} hydrogels at different self-healing times. (e) Self-healing efficiency of PAEG-Zr^{4+} hydrogels.

ered with increasing resting time, which may be due to the dissipation energy generated by the recovery of metal bonds, electrostatic interactions, and hydrogen bonds in the polymer network. In addition, we conducted cyclic stretching experiments under different strains (Fig. 2f and i). During the loading–unloading process, the hysteresis energy and ring area of cyclic stretching increased with increasing tensile strain. During each cycle, the cyclic curves overlapped, which indicated immediate material recovery.

3.3 Self-healing properties

To improve the durability and reliability of the material, hydrogen bonding, metal–ligand bonding and electrostatic interactions were introduced into the polymer network to impart excellent self-healing properties to the composite hydrogel. As shown in Fig. 3a, the dynamic reversible bonds within the PAEG-Zr^{4+} hydrogels were damaged after cutting, and the metal coordination, electrostatic interactions and hydrogen bonds could be rebuilt without any external intervention after the fractured hydrogels were reconnected for a short time, demonstrating the excellent self-healing properties. To highlight our research, we conducted a comparison of the PAEG-Zr^{4+} hydrogels with previously reported materials regarding their self-healing efficiency and time, as shown in Fig. S6b.† The results depicted in the figure demonstrated that the PAEG-Zr^{4+} hydrogels displayed a remarkably efficient and rapid self-healing capacity in comparison with other high-strength hydrogels with self-healing capabilities. Although the hydrogels produced in the reference SR4 could attain a mechanical strength of 7.1 MPa, they are not advantageous for practical use due to their slow repair time. Although the hydrogels synthesized in references SR2 and SR10 exhibit faster self-healing rates, their self-healing efficiency is suboptimal. The healing process of the PAEG-Zr^{4+} hydrogel after cutting is shown in Fig. 3b. The results showed that two parts of hydrogels (one stained with rhodamine B) reassembled together within only 5 min in air (25 °C) and could be stretched arbitrarily. Moreover, we also observed the self-healing process of the fractured hydrogel scratch under microscopy through a stereomicroscope. With the extension of time, the scratch gradually became smaller and repaired, almost disappearing in about 120 min (Fig. 3c). Besides, we conducted tensile tests to further test the self-healing effect of the material. As shown in Fig. 3d and e, as the self-healing time increased, the strain and stress of the PAEG-Zr^{4+} hydrogel were gradually recovered. At about four hours, the stress of the repaired hydrogel after fracture could recover to 93% of the original hydrogel and the strain to 95%. The presence of the dual synergistic effect allowed the PAEG-Zr^{4+} hydrogel to be in working condition for a long time with fast and efficient self-healing ability.

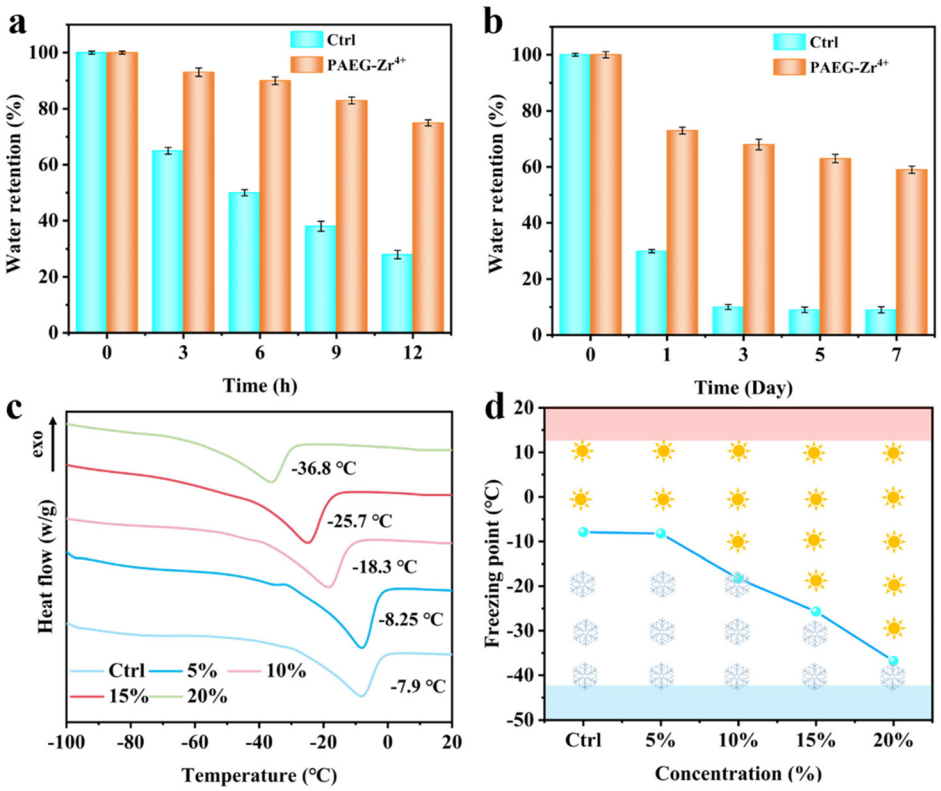

Fig. 4 (a) Moisturizing properties of PAEG-Zr^{4+} hydrogels and control hydrogels stored in air for 12 h. (b) Moisturizing properties of PAEG-Zr^{4+} hydrogels and control hydrogels stored in air for 7 days. (c) DSC test curves of PAEG-Zr^{4+} hydrogels with different glycerol contents. (d) Freezing points of PAEG-Zr^{4+} hydrogels with different glycerol contents.

3.4 Moisturizing and antifreeze properties

Most of the solvents in currently prepared hydrogels are pure water, which may cause the material to lose water at the working temperature. In addition, the water present in hydrogels tends to freeze below zero and lose its deformability, which limits its performance at low temperatures.[40,41] Therefore, a water–glycerol solvent was added to the system as a dispersion medium to synthesize the PAEG-Zr^{4+} hydrogels. To test the moisturizing and anti-freezing effects of PAEG-Zr^{4+}, the glycerol-free hydrogel was also synthesized by the same method. As shown in Fig. 4a, the control hydrogels exposed to air readily lost water within 12 h at room temperature. In contrast, the PAEG-Zr^{4+} hydrogel could retain 79% of its initial water content and maintain almost the same state as the original hydrogel (Fig. S7a†). Simultaneously, the PAEG-Zr^{4+} hydrogel remained in good condition after a week of exposure to air (Fig. 4b). In addition, we performed tensile tests on the hydrogel splines exposed to air for 24 h using a universal testing machine (Fig. S7b†). It is noteworthy that there was a significant increase in stress and a small change in strain in the spline, which may be due to the loss of water in the material.

Based on DSC analysis of the variation of glycerol concentration from 0 to 20 wt% with a concentration gradient of 5 wt%, the phase transition region decreased with the increase of glycerol concentration (Fig. 4c). The freezing point of the PAEG-Zr^{4+} hydrogel could reach as low as −36.8 °C. This phenomenon is caused by the inhibition of ice crystal formation by glycerol,[42,43] which corresponds to the two-phase diagram (Fig. 4d). Fig. S8a† shows the physical diagrams of the PAE-Zr^{4+} and PAEG-Zr^{4+} hydrogels with different storage times at −30 °C. Apparently, the PAE-Zr^{4+} hydrogel had no toughness and became difficult to stretch. In contrast, the PAEG-Zr^{4+} hydrogels were transparent and could be twisted arbitrarily. Furthermore, the mechanical properties of the PAEG-Zr^{4+} hydrogels stored at low temperatures did not change significantly compared with the original hydrogels (Fig. S8b†), which fully demonstrated the excellent antifreeze properties of our prepared materials.

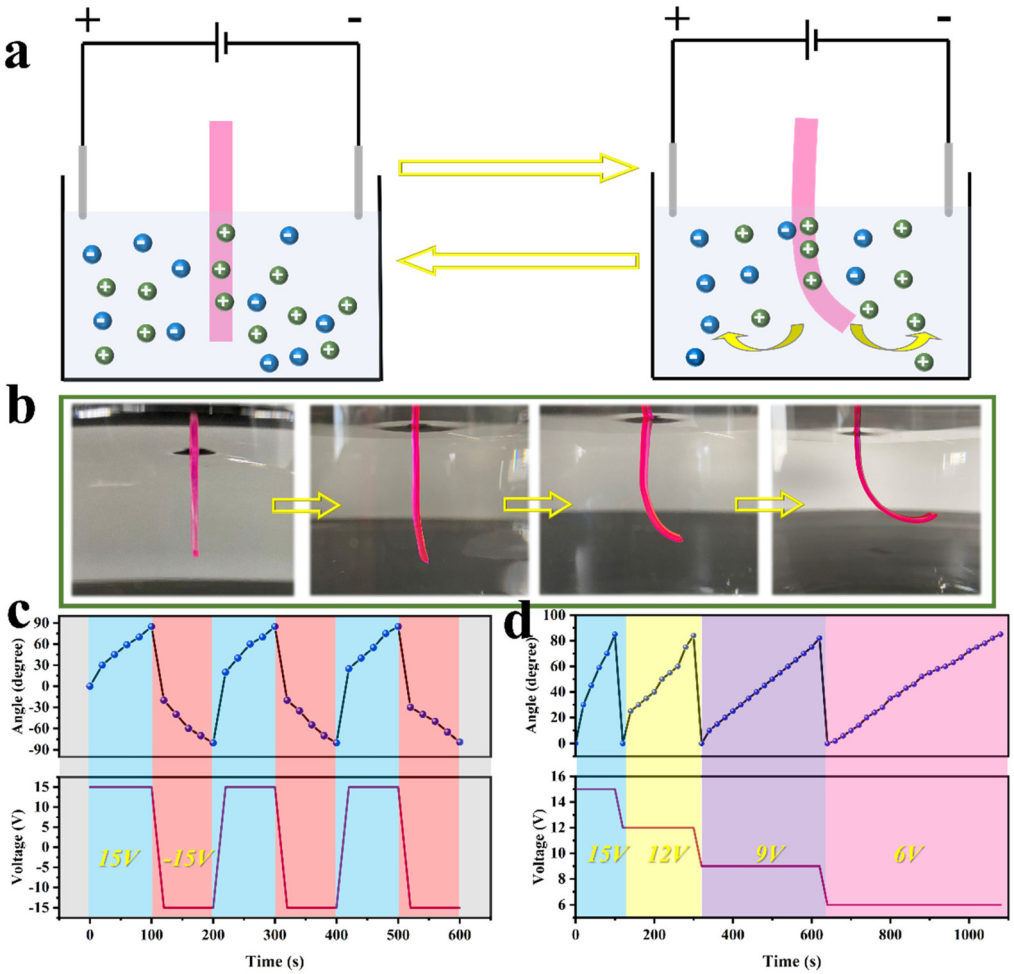

Fig. 5 (a) Electro-responsive actuation of hydrogels. (b) The shape change of the hydrogels during the actuation process. (c) Actuation behavior of hydrogels at voltages of 15 V and −15 V. (d) Actuation behavior of hydrogels at voltages of 6 V, 9 V, 12 V, and 15 V.

3.5 Actuation and shape memory behavior

High-strength hydrogels in the presence of metal ions were used as actuators. As shown in Fig. 5a and b, the stained hydrogel splines were placed in the center of the electric field containing a sodium sulfate solution. After applying an electric field, a hydrogel spline bends to varying degrees. This is attributed to the concentration gradient caused by the movement of ions within the electrolyte solution and the hydrogel, which in turn causes an osmotic pressure difference between the two sides of the hydrogel eventually leading to its bending and swelling.[44] Fig. S9† exhibits the bending angle of hydrogels in the electric field with time, and the sample strip bending angle could reach up to 83°. Since the main network within the hydrogel was constructed by polyacrylic acid, the cations inside the gel migrated to the cathode in the presence of an electric field, resulting in a higher osmotic pressure near the anode side than the other side, which in turn showed a rapid drive of the hydrogel to the cathode. Furthermore, cyclability was a key point for hydrogel actuators. As shown in Fig. 5c, the sample gradually bended under the electric field with a voltage of 15 V, and the maximum angle of 83° could be reached in 100 s. Then the reverse voltage was applied and the hydrogel was bended to 82° towards the other side, which was almost the same as the maximum bending angle formed by the original electric field. In addition, the bending angles of the sample strips in different directions were almost the same after several cycles, which proved that our hydrogel actuator could withstand cyclic bending without damaging the material. Subsequently, we investigated the effect of voltage variation on the actuator. As shown in Fig. S10a and b,† the bending angle of the sample could reach more than 80° under the application of different voltages. At the same time, the response time of the actuator gradually became shorter as the voltage increased. This was due to the fact that the ions moved faster with the increase of voltage leading to a faster response of the driver, which corresponded to the hydrogel driving angle at successively different voltages (Fig. 5d).

PAEG-Zr^{4+} hydrogels could be investigated as shape memory materials due to the property that the polyacrylic acid network coordinated with Zr^{4+} at high temperatures and produced carboxyl aggregation.[45] Therefore, PAEG-Zr^{4+} hydrogels could be deformed by external forces at room temperature, followed by temporary shape fixation at high temperature, and returned to their initial shape in a cold environment (Fig. 6a). In Fig. S11a and c,† the variation of the PAEG-Zr^{4+} hydrogel's shape recovery time with shape fixation time was investigated. We could see that as the fixation time increased, the shape recovery time also increased, which indicated more severe aggregation of polymer chain segments inside the hydrogel. Moreover, we further confirmed the above conclusion by simulating the opening of the petals. As shown in Fig. 6b, the hydrogel was shaped into a bud and then placed in cold water. We could see that three petals (short fixation time) were the

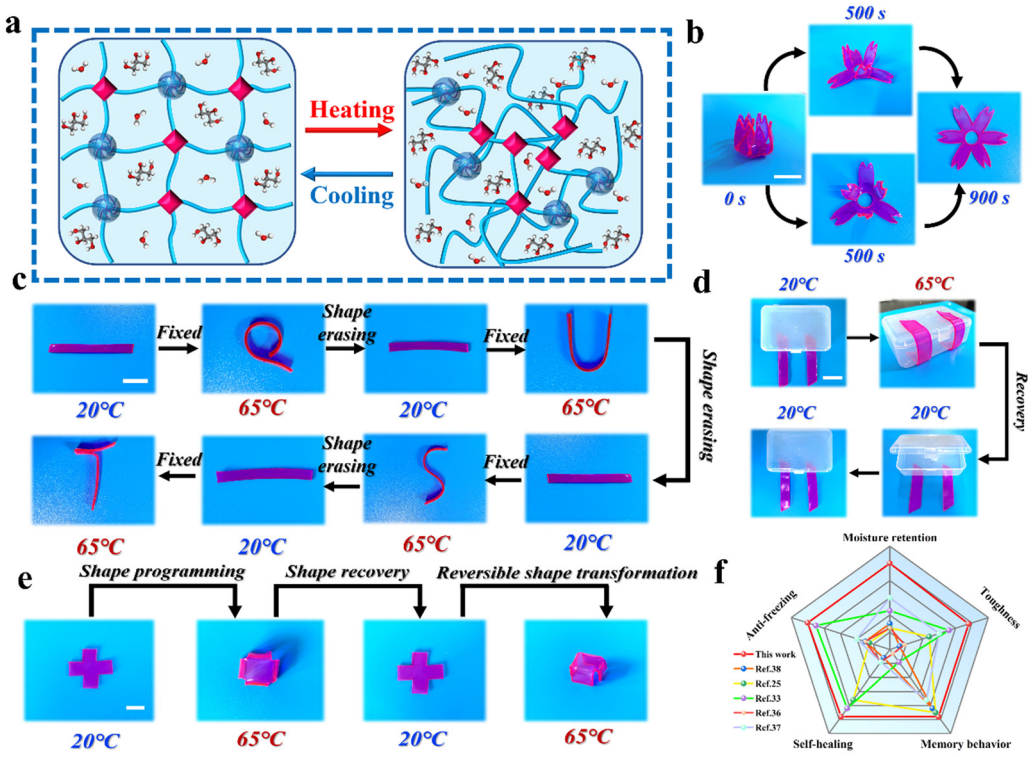

Fig. 6 (a) Shape memory mechanism. (b) The petal-shaped hydrogel simulates the blooming process. (c) Reproducible programmability of the hydrogels. (d) Shape memory hydrogel acts as a protective lock. (e) 2D → 3D shape memory properties of the hydrogel (scale bar = 2 cm). (f) Radar charts compared to other studies in the literature.

first to bloom at 500 s, while at about 900 s, the petals showed full bloom. In addition, we also investigated the circular memory properties of the material. As shown in Fig. S11b, the PAEG-Zr^{4+} hydrogel could reach about 300° in 10 cycles, which fully proved the durability of the material.

Programmability allowed the hydrogel to be reversibly switched between various shapes.[46] As shown in Fig. 6c, the strip-shaped hydrogel could be switched back and forth between randomly shaped letters (such as QUST). This was due to the fact that the hydrogel network reverted from the aggregated state to the original state in the cold environment, and the variation of individual fixed shapes was eliminated, resulting in a programmable effect.[46,47] Furthermore, the switching process of programmable hydrogels inspired us to develop temperature-sensitive security locks. As shown in Fig. 6d, a fixed-shaped hydrogel strip was used to seal the container. The safety lock opened only when the temperature of the container reached a safe temperature. This safety lock design may be applied to the transportation industry. Fig. 6e shows the shape switching of a locally programmed PAEG-Zr^{4+} hydrogel between 1D and 3D (1D → 3D). It is worth noting that this hydrogel can be reprogrammed multiple times and still have good shape transformation effects. In addition, we designed the hydrogel as a catching hand to grasp the model fish (Fig. S12†). The catcher hand could fully grasp the model fish in a 60 °C environment, and then it was placed in a cold environment where the catcher hand slowly returned to its original state and released the object. This interesting application may have a great future in the industrial sector.

Finally, we compared the synthesized hydrogels with previously reported hydrogels in terms of moisture retention, self-healing effect, anti-freezing properties, toughness, and shape memory to demonstrate the superior performance of the materials (Fig. 6f). Under the strong metal–ligand interaction, as well as multiple reversible interactions, the PAEG-Zr^{4+} hydrogels exhibited outstanding mechanical properties, which exceeded the mechanical strength of most reported hydrogel materials. Furthermore, due to the presence of multiple reversible bonds, the PAEG-Zr^{4+} hydrogels showed rapid self-healing capabilities, which enabled the prepared high-strength hydrogel to work for a long time. The anti-freezing and moisturizing properties tackled the issue of low hydrogel tolerance, thus expanding its potential uses in challenging environments. Moreover, the shape memory feature could gradually integrate PAEG-Zr^{4+} hydrogels into the scope of hydrogel-based smart devices of the future.

4 Conclusion

In conclusion, we successfully prepared a composite hydrogel with high toughness, high mechanical strength and excellent self-healing ability based on multiple synergistic interactions. Under the synergistic effects of hydrogen bonding, electrostatic interactions, and metal coordination, the synthesized hydrogels could reach a maximum tensile strength of 6.2 MPa and a toughness of 50 MJ/m^3. Furthermore, the high-strength fractured hydrogel could achieve 95% self-healing within 4 hours. After several rounds of cyclic tensile tests, the PAEG-Zr^{4+} hydrogels demonstrated outstanding fatigue resistance properties due to the rapid reconstruction of multiple reversible bonds within the polymer network. Remarkably, in the presence of glycerol, the PAEG-Zr^{4+} hydrogels exhibited excellent frost protection, withstanding temperatures as low as −36.8 °C while retaining 80% of their water content for up to 12 hours at room temperature. Additionally, composite hydrogels applied in actuator applications could achieve unrestricted shape transformation within various voltage environments. Owing to their sensitivity towards temperature, the PAEG-Zr^{4+} hydrogels proved to be advantageous materials for studying shape memory, programmable properties, and reversible sex-transformation changes, providing valuable insights for the development of hydrogels in the smart materials industry.

Author contributions

Yanqing Wang: conceptualization, methodology, investigation, and writing – original draft. Pengcheng Li: validation, data curation, and software. Shuting Cao: data curation. Yuetao Liu: validation and data curation. Chuanhui Gao: writing – review & editing.

Conflicts of interest

There are no conflicts to declare.

Acknowledgements

The authors thank the National Natural Science Foundation of China (51872150) and the "QingChuang Science and Technology Plan" Project of Colleges and Universities in Shandong Province (2020KJC005).

References

1 G. D. Cha, W. H. Lee, C. Lim, M. K. Choi and D. H. Kim, *Nanoscale*, 2020, **12**, 10456–10473.
2 Z. Zhao, C. Wang, H. Yan and Y. Liu, *Adv. Funct. Mater.*, 2019, **29**, 1905911.
3 X. Duan, J. Yu, Y. Zhu, Z. Zheng, Q. Liao, Y. Xiao, Y. Li, Z. He, Y. Zhao, H. Wang and L. Qu, *ACS Nano*, 2020, **14**, 14929–14938.
4 L. Jia, S. Wu, R. Yuan, T. Xiang and S. Zhou, *ACS Appl. Mater. Interfaces*, 2022, **14**, 27371–27382.
5 M. Wang, H. Zhou, X. Jin, H. Liu, A. Ma, H. Yan, L. Chen and W. Chen, *J. Mater. Chem. C*, 2021, **9**, 1822–1828.
6 C. Yun, S. Hwang and J. Kwak, *Nanoscale*, 2018, **10**, 13581–13588.

7 S. H. Kim, Y. B. Seo, Y. K. Yeon, Y. J. Lee, H. S. Park, M. T. Sultan, J. M. Lee, J. S. Lee, O. J. Lee, H. Hong, H. Lee, O. Ajiteru, Y. J. Suh, S. H. Song, K. H. Lee and C. H. Park, *Biomaterials*, 2020, **260**, 120281.
8 J. Cao, T. Zhang, W. Zhu, H. B. Li and A. G. Shen, *Nanoscale*, 2023, **15**, 11163–11178.
9 Y. Bai and L. Ionov, *Mater. Chem. Front.*, 2022, **6**, 1218–1227.
10 S. Xue, Y. Wu, M. Guo, D. Liu, T. Zhang and W. Lei, *Nanoscale Res. Lett.*, 2018, **13**, 393.
11 S. Xue, Y. Wu, M. Guo, Y. Xia, D. Liu, H. Zhou and W. Lei, *Soft Matter*, 2019, **15**, 3680–3688.
12 D. Zhu, Z. Wang, J. Xie, G. Qu, Q. Yu, Y. Kuai, B. Yu, J. Zheng, Z. Hu and S. Li, *Nanoscale*, 2023, **15**, 10685–10692.
13 X. Li, H. Wang, D. Li, S. Long, G. Zhang and Z. Wu, *ACS Appl. Mater. Interfaces*, 2018, **10**, 31198–31207.
14 L. Zhu, J. Qiu, E. Sakai and K. Ito, *ACS Appl. Mater. Interfaces*, 2017, **9**, 13593–13601.
15 Q. Chen, X. Yan, L. Zhu, H. Chen, B. Jiang, D. Wei, L. Huang, J. Yang, B. Liu and J. Zheng, *Chem. Mater.*, 2016, **28**, 5710–5720.
16 W. He, X. Guo, P. Xia, S. Lu, Y. Zhang and H. Fan, *J. Colloid Interface Sci.*, 2023, **647**, 456–466.
17 J. Mo, Y. Dai, C. Zhang, Y. Zhou, W. Li, Y. Song, C. Wu and Z. Wang, *Mater. Horiz.*, 2021, **8**, 3409–3416.
18 T. Long, Y. Li, X. Fang and J. Sun, *Adv. Funct. Mater.*, 2018, **28**, 1804416.
19 X. Dai, Y. Zhang, L. Gao, T. Bai, W. Wang, Y. Cui and W. Liu, *Adv. Mater.*, 2015, **27**, 3566–3571.
20 Z. Zhao, K. Zhang, Y. Liu, J. Zhou and M. Liu, *Adv. Mater.*, 2017, **29**(33), 1701695.
21 L. Zhao, B. Wang, Z. Mao, X. Sui and X. Feng, *Chem. Eng. J.*, 2022, **433**, 133500.
22 X. Sui, H. Guo, C. Cai, Q. Li, C. Wen, X. Zhang, X. Wang, J. Yang and L. Zhang, *Chem. Eng. J.*, 2021, **419**, 129478.
23 X. Yang, M. Guo, Y. Wu, S. Xue, Z. Li, H. Zhou, A. T. Smith and L. Sun, *ACS Appl. Mater. Interfaces*, 2020, **12**, 56445–56453.
24 T. Yuan, X. Cui, X. Liu, X. Qu and J. Sun, *Macromolecules*, 2019, **52**, 3141–3149.
25 S. M. Kim, H. Jeon, S. H. Shin, S. A. Park, J. Jegal, S. Y. Hwang, D. X. Oh and J. Park, *Adv. Mater.*, 2018, **30**, 1705145.
26 Y. Zhu, K. Kang, J. Jia, S. Wang and J. Wang, *Nanoscale*, 2023, **15**, 9823–9834.
27 W. P. Chen, D. Z. Hao, W. J. Hao, X. L. Guo and L. Jiang, *ACS Appl. Mater. Interfaces*, 2018, **10**, 1258–1265.
28 X. Yang, G. Liu, L. Peng, J. Guo, L. Tao, J. Yuan, C. Chang, Y. Wei and L. Zhang, *Adv. Funct. Mater.*, 2017, **27**, 1703174.
29 S. Xue, Y. Wu, G. Liu, M. Guo, Y. Liu, T. Zhang and Z. Wang, *J. Mater. Chem. A*, 2021, **9**, 5730–5739.
30 X. Fang and J. Sun, *ACS Macro Lett.*, 2019, **8**, 500–505.
31 Z. Deng, R. Yu and B. Guo, *Mater. Chem. Front.*, 2021, **5**, 2092–2123.
32 H. C. Yu, X. P. Hao, C. W. Zhang, S. Y. Zheng, M. Du, S. Liang, Z. L. Wu and Q. Zheng, *Small*, 2021, **17**, 2103836.
33 J. Zhao, X. Xi, H. Ouyang, J. Yang, Y. Wang, L. Yi, D. Song, Y. Song and L. Zhao, *Carbohydr. Polym.*, 2021, **272**, 118445.
34 X. Dai, J. Wang, F. Teng, Z. Shao and X. Huang, *J. Polym. Sci., Part B: Polym. Phys.*, 2019, **57**, 981–991.
35 J. Gu, J. Huang, G. Chen, L. Hou, J. Zhang, X. Zhang, X. Yang, L. Guan, X. Jiang and H. Liu, *ACS Appl. Mater. Interfaces*, 2020, **12**, 40815–40827.
36 Y. Xia, Y. Wu, T. Yu, S. Xue, M. Guo, J. Li and Z. Li, *ACS Appl. Mater. Interfaces*, 2019, **11**, 21117–21125.
37 Y. Wang, M. Zheng, X. Wang, S. Li and J. Sun, *ACS Appl. Mater. Interfaces*, 2018, **10**, 30716–30722.
38 F. Li, G. Zhang, Y. Xia, Z. Wang, H. Jiang, X. Feng, Y. Zhang, M. Liu and H. Li, *Compos. Sci. Technol.*, 2018, **165**, 339–346.
39 R. Liang, Z. Li, L.-T. Weng, L. Zhang and G. Sun, *Mater. Chem. Front.*, 2018, **2**, 2076–2080.
40 H. Gao, Z. Zhao, Y. Cai, J. Zhou, W. Hua, L. Chen, L. Wang, J. Zhang, D. Han, M. Liu and L. Jiang, *Nat. Commun.*, 2017, **8**, 15911.
41 X. Xie, X. Xu, Q. Zhu, S. Lu, Y. Li and Y. Bai, *Mater. Chem. Front.*, 2022, **6**, 1973–1981.
42 Y. Wang, B. Pang, R. Wang, Y. Gao, Y. Liu and C. Gao, *Composites, Part A*, 2022, **160**, 107039.
43 Y. Wang, P. Chen, X. Zhou, Y. Liu, N. Wang and C. Gao, *ACS Appl. Mater. Interfaces*, 2022, **14**, 47100–47112.
44 H. Jiang and J. Tang, *ACS Appl. Polym. Mater.*, 2020, **2**, 3821–3827.
45 L. Hua, C. Zhao, X. Guan, J. Lu and J. Zhang, *Sci. China Mater.*, 2022, **65**, 2274–2280.
46 K. Liu, Y. Zhang, H. Cao, H. Liu, Y. Geng, W. Yuan, J. Zhou, Z. L. Wu, G. Shan, Y. Bao, Q. Zhao, T. Xie and P. Pan, *Adv. Mater.*, 2020, **32**, 2001693.
47 N. Zhao, Z. Yu, J. Huang, Y. Liu, Y. Zhao, X. Fu, P. Yang and K. Liu, *Nanoscale*, 2023, **15**, 6179–6186.